Front. Optoelectron. 2016, 9(3): 466–482
DOI 10.1007/s12200-016-0558-7

REVIEW ARTICLE

Integrated liquid crystal photonic bandgap fiber devices

Kaiwei LI, Ting ZHANG, Nan ZHANG, Mengying ZHANG, Jing ZHANG, Tingting WU, Shaoyang MA, Junying WU, Ming CHEN, Yi HE, Lei WEI (✉)

School of Electrical and Electronic Engineering, Nanyang Technological University, Singapore 639798, Singapore

Abstract Liquid crystal photonic bandgap (LCPBG) fibers provide a versatile and robust platform for designing optical fiber devices, which are highly tunable and exhibit novel optical properties for manipulation of guided light. We review the research progress on design, fabrication and development of integrated LCPBG fiber devices.

Keywords photonic crystal fibers (PCFs), fiber devices, liquid crystal (LC) devices

1 Introduction

Photonic crystal fibers (PCFs) have been the main focus of fundamental fiber research over the last decade due to their unique optical properties and a much higher degree of design freedom compared to conventional optical fibers [1–3]. More applications using PCFs have been found in fiber-optic communications, fiber sensors, fiber lasers, and other areas. PCFs are characterized by an arrangement of micron-sized air-holes running along the length of the fiber. The microstructure allows the realization of so-called index-guiding PCFs, which guide light in a high-index core using a principle similar to total internal reflection (TIR), and photonic bandgap (PBG) guiding PCFs, which can guide light in a low-index core. An initial index-guiding PCF can be converted to a PBG-guiding PCF by infiltrating the air holes with high-index liquid materials [4,5]. A very interesting class of liquid materials for this purpose is liquid crystals (LCs), due to their high thermo-optic effects, complex alignment patterns and large dielectric anisotropy. In this paper, we review the research progress of integrated liquid crystal photonic bandgap (LCPBG) fiber devices.

Received November 11, 2015; accepted December 30, 2015

E-mail: wei.lei@ntu.edu.sg

2 Liquid crystal photonic bandgap fibers

Tunable all-in-fiber devices are promising candidates for creating compact devices, which are widely applied in fiber-based systems [6]. LCs are materials offering highly interesting possibilities for designing tunable optical devices, and the presence of the air-holes in PCFs makes them good hosts for LCs.

2.1 Liquid crystal infiltration

Infiltrating LCs in PCFs can be achieved by using capillary forces, vacuum or pressure [5,7,8]. For short infiltration length, using capillary forces is a simple and effective method leading to a homogeneous alignment without orientational defects which is important to achieve low scattering losses. A drop of LC is positioned on a clean glass plate and the tip of the PCF is dipped into the LC drop. A visible laser diode is coupled into the other end of the fiber, and the laser light is scattered in the filled section to indicate the length of the filling. Typical infiltration length for LCPBG devices is $1-2$ cm. Infiltrating LCs using pressure or vacuum requires to place one fiber end into a pressure or vacuum chamber. The LCs are then pushed or pulled into the PCF which accelerates the infiltration process compared to capillary force driven infiltration. This is useful for longer infiltration lengths, since the infiltration process considerably slows down for increasing infiltration time when using capillary forces based infiltration. The main disadvantage of these methods is that orientational defects can be introduced, resulting in stronger scattering and therefore additional losses in the transmission spectrum of the LCPBG fibers [7].

The infiltration temperature is also an important factor influencing the final alignment of the LC and the losses of the LCPBG fibers. For nematic planar aligned LCs, such as E7 (Merck, Germany), it is found that the best alignment can be achieved by processing the infiltration in their isotropic phase. Before infiltration the LCs are heated up until the isotropic phase is reached, and kept at this

temperature until the end of the infiltration process. The quality of the alignment could further be improved by slowly cooling the LCs down after the infiltration and then heating them once more to isotropic phase and cooling them down afterwards. This technique results in optimized scattering losses of the LCPBG fiber [9,10]. For nematic splayed aligned LCs, such as MDA-00-3969 or MLC-6608 (Merck, Germany), on the contrary, it has been observed that the alignment is deteriorated when they are infiltrated in their isotropic phase and therefore their infiltration process is preferred to be carried out at room temperature [11,12].

2.2 Alignment of liquid crystals

The type of alignment of LCs in cylindrical capillaries, planar or splayed, is determined by their boundary alignment. The boundary alignment is influenced by many factors, for example, smoothness of the surface, surface tension, elastic constants, dielectric anisotropy, dipole and rigidity of the LC molecules [13]. Therefore, it is important to know how the LC molecules are aligned inside the circular capillaries of the fiber cladding. Polarization microscopy is not suitable to investigate the LC alignment of LCPBG fibers due to the scattering effects from many capillaries that define the cladding structure. Instead, single LC infiltrated glass capillary is used that is made of the same material and produced by using the same technique as the PCFs. It has been demonstrated that glass capillaries of dimension $2-6$ μm infiltrated with LCs present a good alignment [14]. Such an investigation of the alignment is done by filling a single capillary with the LC, placing the capillary on a rotatable plate between two crossed polarizers and looking at it through a microscope. White light is launched through the setup, and due to the crossed polarizers no light can be transmitted. Only if a birefringent medium is placed between two polarizers, light can be transmitted. If the LC molecules are aligned parallel to either of the polarizers, no light will be transmitted. If the LC molecules are aligned at an angle, the polarized light will see both the ordinary and extraordinary indices which will turn the polarization of the light, allowing it to pass through the second polarizer. By observing the light pattern after the second polarizer, it is able to determine the alignment of the LC molecules. Normally, two pictures at two different angles (0° and 45°) of the sample with respect to the polarizer are sufficient to determine the alignment.

Figure 1 shows the images of LC alignment at two different angles (0° and 45°) in different configurations. E7 shows a planar alignment in Figs. 1(a) and 1(b), where all molecules are parallel to the capillary axis. The infiltration of E7 is done in its isotropic phase. MDA-00-3969 is splay-aligned with a 45° boundary alignment at the boundary of the capillary and parallel alignment in the center, as shown in Figs. 1(c) and 1(d). MLC-6608 is also splay-aligned, but with a 90° boundary alignment and parallel alignment in the center, as shown in Figs. 1(e) and 1(f). By coating the inner surface of the capillaries with a surfactant, the alignment of LCs can be modified due to the change of the surface anchoring conditions. A perpendicular boundary alignment can be achieved by coating the surface with lecithin [15], which is a polar molecule widely used as an emulsifier in the food industry. The main advantage of modifying planar aligned LCs to splay-aligned is to design continuously tunable LC devices with much lower Fredericks threshold, compared to planar aligned LCs.

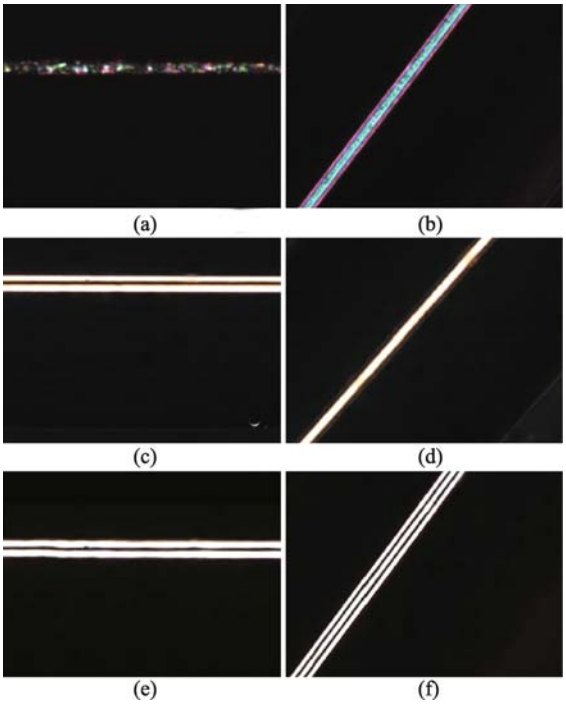

Fig. 1 Polarization optical microscopy images of different LCs in a single capillary. (a) and (b) E7; (c) and (d) MDA-00-3969; (e) and (f) MLC-6608 [10–12]

2.3 Transmission spectrum and losses

As an example, a solid-core LMA PCF (LMA-13, NKT Photonics A/S, Denmark) with four rings of air-holes is used, with the hole diameter, pitch and outer fiber diameter of 4.3, 8.5 and 125 μm, respectively. The LC is MDA-00-3969 (Merck, Germany), with a wavelength dependent ordinary and extraordinary refractive index of $n_o = 1.50$ and $n_e = 1.72$ at 589 nm. The filling length is 10 mm and the spectrum is measured at room temperature. The transmission spectrum is shown in Fig. 2.

The PBG guiding mechanism can be explained either by the anti-resonant reflecting optical waveguides (ARROW) model [16] or by the coupled mode theory [17]. These

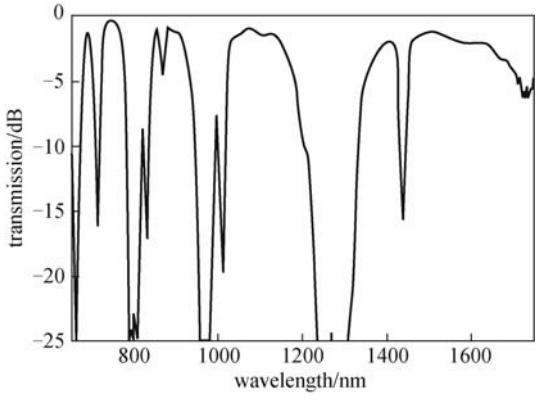

Fig. 2 Transmission spectrum of LMA-13 fiber filled with MDA-00-3969

methods have also been applied to estimate the spectral position of the bandgaps [18–20]. Guiding light in a low-index core can be described in terms of anti-resonant scattering of the light at surrounding dielectric optical cavities. At resonance those cavities are transparent and light will escape from the core, while for wavelengths between resonances light is reflected back and in this way confined to the core. ARROW model was first considered with planar geometries [21], where the high-index cladding constituted a Fabry-Perot like resonator. Similar arguments were later on used for a cladding structure consisting of dielectric cylinders [16,22–24]. With the high refractive index inclusions, the filled holes form isolated cladding waveguides. The allowed states of the cladding waveguide form bands of super modes, which split up in effective index and bandgaps are formed between the bands. First band contains coupled states of LP_{01} modes, second band contains coupled states of LP_{11} modes, etc. When the high refractive index inclusions are anisotropic, in this case LCs, the individual bands of super modes further split up due to the different electric field distributions of transverse electric (TE), transverse magnetic (TM) and hybrid modes. New and narrow bandgaps can be formed [25]. The notch appearing in the transmission spectrum is caused by a cladding mode crossing a bandgap, forming a so-called "avoided-crossing" with the core mode of the bandgap [26].

The insertion loss of this LCPBG fiber is around 2 dB at 1550 nm in the middle of the bandgap. Some factors can contribute this loss, for example, absorption and scattering from LCs and silica, coupling loss between the TIR mode of the unfilled fiber and the PBG mode of the filled fiber, and propagation loss. Absorption and scattering losses of nematic LC are generally much larger than those of silica, and the losses from silica can, therefore, be ignored over such short lengths. Furthermore, the LC scattering losses are around 15 – 40 dB/cm and much larger than the LC absorption losses [27]. Therefore, the absorption losses can be neglected. It has also been shown that the scattering loss of nematic LCs can be decreased substantially by confining the LC in small capillaries with inner diameters of 2.8 μm, and losses of 1 – 3 dB/cm have been reported [7]. Leakage loss arises since the cladding structure is finite and the guided mode may penetrate the microstructured cladding and leak into the outer cladding region. The leakage loss is strongly dependent on the number of rings surrounding the core [28]. The coupling loss between the TIR mode of the unfilled fiber and the PBG mode of the filled fiber has been found to be the main source, which is originated from a mismatch in mode profiles [25].

3 Integrated liquid crystal photonic bandgap fiber devices

The unique property of LCs, compared with other high-index liquids, is their large electro-optic effect, which allows for electrically driven LCPBG fiber devices for switching [10], or as tunable polarization controllers [11]. However, the reported LCPBG fiber devices are demonstrated in principle on fiber coupling stages and the electric field is applied by using bulk metal plates, which are not stable and portable to be inserted in actual systems, and consequently limit the practical applications of these all-in-fiber devices. A critical issue for most applications is the fiber based compact design and packaging, where the LCPBG fiber is connected with patch cables. The LCPBG fiber is filled from one end and preferably not repositioned, and standard arc-fusion splicing cannot be achieved, because LCs can be burnt at high temperature and LC residues can contaminate the end facets of the fibers. Instead, a self-aligned packaging method for LCPBG fiber devices based on on-chip V-grooves and electrodes has been realized [29,30].

3.1 Fabrication of integrated LCPBG fiber devices

Since an external applied electrical field reorients the alignment of LC and breaks the symmetry of the LCPBG fiber structure, it is desirable to control the electric field in a more flexible way in order to control the optical axis of the device. An integrated on-chip design is demonstrated, as shown in Fig. 3(a). This compact design not only enables the LCPBG fiber devices more easily applied in fiber based systems, but also can be used as a standard platform to develop LCPBG fiber devices for different applications. A LCPBG fiber is mounted between two V-grooves fabricated in a silicon substrate by standard UV lithography and KOH wet etching techniques. Two single mode fiber (SMF) pigtails are fixed in the grooves at each end of the LCPBG fiber for coupling in and out of the device. Gold electrodes are deposited on the side walls of the grooves, forming a set of electrodes, which fix the fiber at four orthogonal corners relative to the core. The electrodes are electrically isolated from the silicon substrate by a thermal

oxide layer, and a titanium layer (10 nm) is used as an adhesion layer between the gold layer and the oxide. The assembly is sealed with epoxy, and the top and bottom sides of the device are electrically grounded. The electric connection is made by wire-bonding. Figure 3(b) illustrates the scanning electron microscope (SEM) image of the cross-section of the fabricated device.

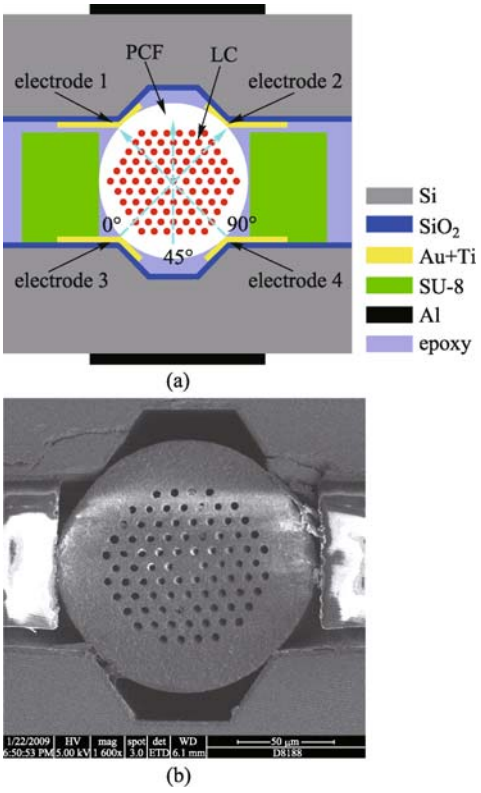

Fig. 3 (a) Cross-section of the LCPBG fiber device. Dotted lines show the direction of electric field effectively applied to the LCPBG fiber; (b) SEM image of the fabricated device [30]

To minimize the misalignment of fiber coupling and subsequently reduce the total insertion loss of the device, SU-8 fiber fixing structures are built up on the electrodes. The height of each structure is 80 μm, since the space between top and bottom chips is $D/1.414 = 88.4$ μm, where D is the outer diameter of the fiber (D = 125 μm). The distance between two neighboring structures is 126 μm, taking the small variation of the fiber outer diameter into account. These SU-8 structures also act as the spacers between the top and the bottom chips along the whole device to avoid tilting the electrodes.

Using the four electrodes it is possible to control the direction of the electric field in the transversal direction and thereby the transversal orientation of the LC molecules, in this way obtaining one more degree of freedom in controlling the device. The device is driven in bipolar mode by using two 1 kHz sine wave signals Vs, −Vs. The device electrodes are connected in different electrode configurations (ECs) corresponding to three directions of the electric field (0°, 45°, and 90°) as the dotted lines shown in Fig. 3(a).

EC1 (0°): electrode 1 = −Vs, electrode 4 = Vs.

EC2 (45°): electrode 1 = electrode 2 = −0.707 Vs, electrode 3 = electrode 4 = 0.707 Vs.

EC3 (90°): electrode 2 = −Vs, electrode 3 = Vs.

3.2 Tunable and rotatable polarizers

For planar aligned LCs, small thermal fluctuations of the LCs cause a little tilt. Depending on the direction of the tilt, the LCs will orient in either of two directions. Most of the molecules reorient into the same direction but there are also areas where the orientation is opposite. They are called reverse tilt domain defects, which define point scatters caused by a non-homogeneous reorientation which result in a strong attenuation of the transmission spectrum. Taking advantage of this effect, tunable and rotatable polarizers have been demonstrated as below.

The fiber used in the experiments is LMA-10, (NKT Photonics A/S, Denmark), with a solid-core surrounded by 7 rings of air-holes arranged in a triangular lattice. The hole diameter, inter-hole distance and outer fiber diameter are 3.1, 7.2 and 125 μm, respectively. The LC is E7 (Merck, Germany) with wavelength dependent ordinary and extraordinary refractive index of $n_o = 1.52$ and $n_e = 1.75$ at 589.3 nm. The LC E7 is infiltrated for 10 mm of the length of the fiber by using capillary forces.

The performance of this device is tested using a broadband polarizer and three achromatic wave plates (quarter, half, quarter, 1200 – 1650 nm) coupled to the light from a supercontinuum source (SuperK, NKT Photonics A/S, Denmark) to have a full broadband polarization control. The device is driven in bipolar mode by using two 1 kHz sine wave signals Vs, −Vs. The 1 kHz sine wave driving voltage Vs for the device is generated by a signal generator and the phase-shifted signal −Vs is generated by an inverter. Vs and −Vs are amplified using high voltage amplifiers and the DC components of Vs and −Vs are removed by high-pass filters. The transmission spectrum is measured by an optical spectrum analyzer, and normalized to the spectrum without inserting the device. Figures 4(a) – 4(c) plot the normalized transmission spectra of the polarizer at 0 Vrms together with the polarization dependent transmission spectra for EC1, EC2 and EC3 at the effective driving voltage of 50 Vrms. These figures show that the bandgaps become highly polarized when the electric field is applied and that the principal axis of the polarizer can be rotated in steps of 45°. The transmission axis of the polarizer is aligned orthogonal to the direction of the electric field, and the increased loss of the optical mode polarized along the electrical field direction is caused by a combination of two effects: first, the effective mode index of the cladding states belonging to the short-wavelength bandgap edge mode is pushed up and into

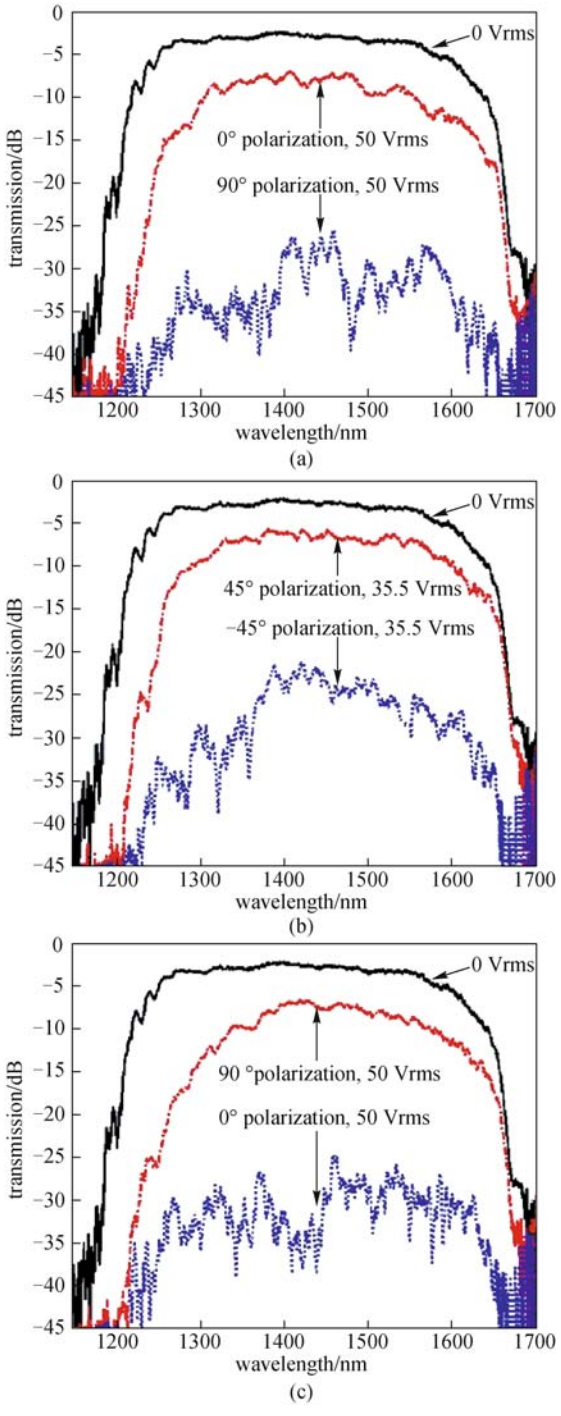

Fig. 4 Normalized transmission spectra of the polarizer at 0 Vrms together with the polarization dependent transmission spectra for different ECs. (a) EC1, (b) EC2, and (c) EC3 at the effective driving voltage of 50 Vrms [30]

the bandgap, causing polarization dependent coupling of the core mode to these cladding states. This occurs mainly around the short-wavelength part of the bandgap, causing an increased loss for both polarizations. The short-wavelength PBG edge is therefore also slightly red-shifted due to this. Second, as mentioned before, the reorientation of the LC molecules along the field direction causes polarization-dependent scattering appearing from reverse tilt domain defects. These defects result in a strong attenuation of the transmission spectrum. The device has the potential as a compact and low cost polarimeter together with a wave plate for polarization monitoring of high speed optical communication systems or for fiber-optic sensors.

A larger activation loss has to be addressed in application systems when a higher polarization extinction ratio is required. With the driving voltage of 50 Vrms, EC1 and EC3 have almost the same polarization extinction ratio of around 21 dB, but 19.1 dB for EC2. Also, the activation loss is equal for EC1 and EC3 but 0.8 dB lower for EC2. These differences are probably caused by the variations of electric field distribution within the PCF between EC1, EC3 and EC2, since the air-holes with LC are arranged triangularly in the transversal plane and the electric field distribution depends on the angular rotation of PCF with respect to the direction of electric field where the LC region is covered. The polarization extinction ratio is continuously tuned when the driving voltage is above a threshold at 32 Vrms in this case. This threshold is named Fredericks transition to balance the elastic free-energy density and the contribution to the free-energy density given by the electric field.

3.3 Tunable long-period grating devices

Long-period gratings (LPGs) inscribed in optical fibers resonantly couple light from the core mode to a cladding mode of the fiber [31]. The coupling occurs at the resonance wavelength, which is the wavelength of phase match between the core mode and the co-propagating cladding mode. When the phase matching condition is satisfied, the power can be transferred from the core mode to a lossy cladding mode and a loss peak in transmission appears. LPGs have a wide range of applications, for example, optical filtering [31], gain equalization [32], mode conversion [33], temperature or strain sensors [34], and biochemical sensing [35].

Many approaches have been reported to form LPGs in PCFs, such as CO_2 laser writing [36], electric-arc discharges [37], mechanical pressure [38], and femtosecond laser irradiation [39]. It is difficult to obtain stable and both strength and wavelength tunable LPGs by using these approaches. On the other hand, the presence of air-holes in PCFs gives the possibility to fill them with liquid materials, and this provides more methods to achieve LPGs. Tunable acoustic LPGs in high index fluid filled PBG fibers have been realized [40], but the bulky radio frequency (RF) signal generation has to be considered for practical applications. Furthermore, electrically induced LPGs in LCPBG fibers have also been investigated by using the

high electro-optic effect of LCs [41]. However, both the strength and electrical tunability of the loss peaks are highly limited, due to the large irregular variation of the periodic metal electrodes induced by machining process. Here, an on-chip tunable LPG device by integrating LCPBG fiber on the compact platform is achieved.

The fiber used in the experiments is LMA-10 (NKT Photonics A/S, Denmark), and LC is E7 (Merck, Germany). A 20 mm long LMA-10 fiber is filled with LC E7 by using capillary forces, and then integrated into the compact package as illustrated in Fig. 5(a). The grating pitch is 800 μm defined by a 400 μm wide comb shaped Au electrode and a 400 μm wide SiO_2 spacing as illustrated in Fig. 5(b). The device is driven by 1 kHz sine wave signal. Broadband unpolarized light from a supercontinuum source (SuperK, NKT Photonics A/S, Denmark) is coupled into this device. The transmission spectrum is measured by an optical spectrum analyzer, and normalized to the transmission spectrum without inserting the device. Figure 6(a) plots the transmission bandgap in the wavelength range 1100 – 1660 nm with and without the applied voltage. The temperature is fixed at 25°C and no pressure is applied to the device. One distinct loss peak is visible at 1471 nm. When the driving voltage increases, this peak becomes deeper. Under 70 Vrms, the strength of the loss peak is 14.7 dB and the activation loss in the middle of the bandgap is 1.9 dB. There is no memory effect of this LPG device, i.e., the loss peak completely disappears, when the voltage is turned off. The spectral position of the loss peak can be further shifted to required wavelengths by tailoring the dimensions of the PCFs and the grating pitch, thereby

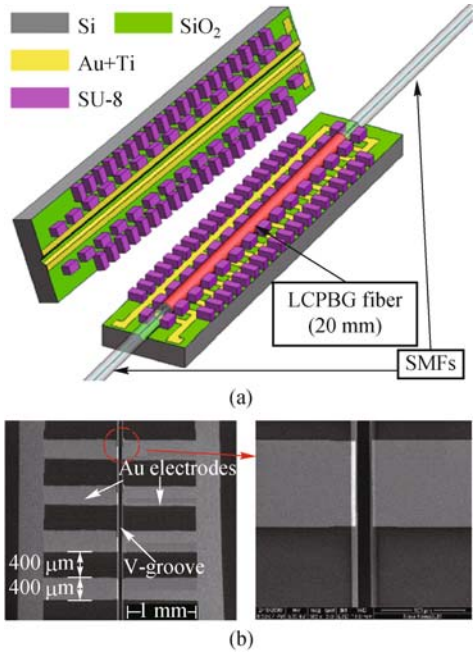

Fig. 5 (a) Chip assembly of the LPG device; (b) SEM image of the fabricated device [69]

realizing an optical component that can be easily integrated in optical systems, which also shows the high degree of freedom in designing LCPBG fiber devices.

By tuning the temperature of the LCs, their refractive indices change and the position of the loss peak can therefore be tuned. The spectral position of the loss peak at 1471 nm as a function of temperature is shown in Fig. 6(b). The peak moves toward shorter wavelengths when the temperature is changed from 25°C to 40°C, and toward longer wavelengths from 40°C to 59°C. This shift can be explained by the change in the refractive indices of E7 as a function of temperature as shown in the inset of Fig. 6(b). The shift of the resonance wavelength is mainly determined by the ordinary refractive index of LC, because the electric field is mostly in this direction. Below 40°C, the gradient of the ordinary index of E7 is almost zero, while the extraordinary index decreases as a function of temperature. Above 40°C, the ordinary index starts to increase and, since the resonance wavelength is mostly affected by this, the loss peak starts to move toward longer wavelengths. During the thermal tuning process, the shape of the loss peak is slightly changed.

The dynamic response of the LCPBG fiber devices is determined by the dynamic properties of the LC. When the voltage is applied, the dynamics is a balance between the dielectric torque and the viscous torque working against any reorientation. When the applied voltage is removed, the LC relaxes back to the equilibrium, and the dynamics is determined by a balance between the viscous torques and the elastic torques, trying to pull the molecules back to equilibrium [42]. Switching is performed by amplitude modulating the 1 kHz sine signal with 50% duty cycle by a 5 Hz square signal. When there is no applied electric field, there is high transmission at 1471 nm. When an electric field above the Fredericks threshold is applied, the loss peak appears and the transmission at this wavelength is low. A photodiode is used to detect the intensity of the light at the output of the device and an oscilloscope displays the photodiode voltage. The rise and decay time t_{on} and t_{off} are measured from 10% to 90% of the amplitude modulation, and shown in Fig. 6(c) as a function of the driving voltage. t_{off} converges toward 11.6 ms and is weakly dependent on the driving voltage. t_{on} is from 15.5 to 8.8 ms and strongly dependent on the driving voltage, as expected.

3.4 Tunable and rotatable polarization controllers

Controlling the state of polarization has become an important consideration in fiber-optic communication and optical sensing systems. Some methods for achieving polarization transformations have been developed, such as mechanical squeezing of fibers [43], rotating wave plates [44], electro-optic crystal waveguides [45], and LC retarders [46]. With the recent development of PCFs, birefringence control has been proposed by using thermal tuning of the refractive index of a polymer partially

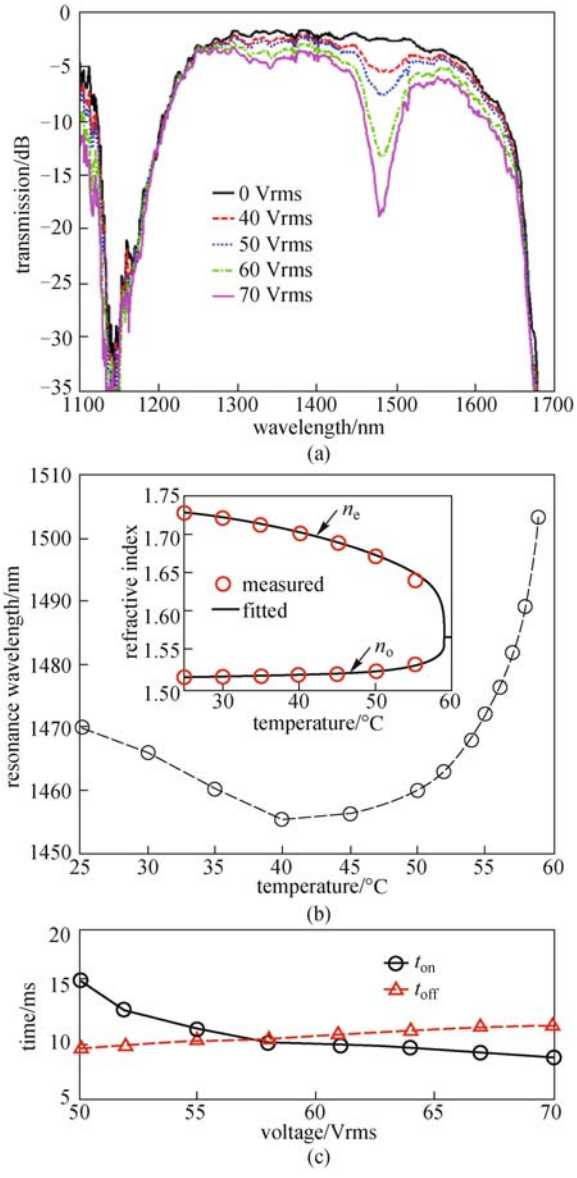

Fig. 6 (a) Transmission bandgap in the wavelength range 1140–1660 nm with and without the voltage by using unpolarized light; (b) spectral position of the loss peak at 1471 nm as a function of temperature. The inset shows the change of the refractive indices of E7 as a function of temperature; (c) measured response time as a function of driving voltage [69]

infiltrated in some of the air-holes of PCF [47]. Polarization controllers and polarization switches are also demonstrated by using microstructured fibers equipped with internal electrodes [48].

Under the application of an electric field, because of the reorientation of the LC, the bandgap shift becomes polarization dependent. The guided modes (eigenstates) loose their degeneracy and experience a different phase delay when propagating through the LCPBG fiber. This opens up the possibility of tuning the birefringence of the structure by applying an external electric field, therefore realizing the all-in-fiber electrically driven tunable polarization controllers. Among the available LCs, the splay-aligned ones are the most appropriate to be used for the fabrication of tunable polarization controllers. In fact, these LCs, as previously discussed, do not have a Fredericks transition threshold and do not exhibit reverse tilt domain defects as planar aligned LCs. In planar aligned LCs, due to the thermal fluctuations, the director can tilt in two different directions when an electric field is applied to the LC, causing orientational defects at the border between two reverse tilt domains. Such defects cause a local change of the refractive index which introduces voltage dependent loss, also called activation loss. In tunable polarization controllers, the loss of the device should preferably be constant and not dependent on the applied voltage. Therefore, splay-aligned LCs are the most suitable ones for the fabrication of polarization controllers. The fiber used in the experiments is LMA-13 (NKT Photonics A/S, Denmark). A negative dielectric LC is used, MLC-6608 (Merck, Germany), which has a wavelength dependent ordinary and extraordinary refractive index of n_o = 1.47 and n_e = 1.55 at 589.3 nm. The LC MLC-6608 is infiltrated for 20 mm of the length of the fiber by using capillary forces, and then integrated into the compact package.

When an electric field is applied to the LCPBG fiber, the LC reorients depending on the direction and strength of the applied voltage. The two orthogonally polarized guiding modes in LCPBG fiber experience different refractive indices compared to the case in which the field is off, and this introduces a phase shift between them. To measure the electrically induced phase shift and corresponding birefringence change, a polarized and tunable laser source operating from 1520 to 1620 nm is used. A polarization analyzer launches the light in the LCPBG fiber device and resolves the output light into the Stokes parameters, which are plotted on the surface of the Poincare sphere. Actively controlled phase shift between the orthogonal polarizations in the device results in a corresponding rotation in the sphere. To achieve a tunable device with low activation loss when the electric field is applied, 210 Vrms has been considered as the maximum driving voltage and the maximum activation loss of 0.45 dB is found.

Figures 7(a)–7(e) show the electrically induced phase shift in the Poincare sphere for EC1 when a driving voltage from 90 to 210 Vrms is applied to the device at 30°C by launching 1550 nm polarized laser light. The red line represents the polarization states in the near part of the sphere and the blue line represents the polarization states on the opposite side of the sphere. Figure 7(f) shows the phase shift in the Poincare sphere for EC1, EC2 and EC3 with the driving voltage of 210 Vrms. The same measurement has been taken for 35°C and 40°C. When the temperature increases, the electrically induced phase shift decreases. This is because the birefringence of LC decreases as a function of temperature until it becomes zero at the clearing temperature. These results demonstrate

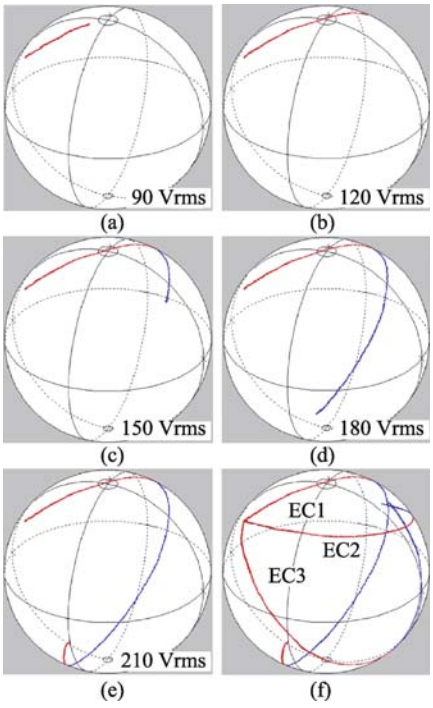

Fig. 7 (a)–(e) Phase shift in the Poincare sphere for EC1 when a driving voltage from 90 to 210 Vrms is applied to the device at 30°C by launching 1550 nm polarized laser light; (f) phase shift in the Poincare sphere for EC1, EC2 and EC3 with the driving voltage of 210 Vrms [70]

that the device can find use as a continuously tunable polarization controller, but also can act as a quarter-wave plate with 90° phase shift and a half-wave plate with 180° phase shift. Since the electrically induced phase shift is wavelength dependent, small variations of the driving voltage are required to develop high performance polarization controllers or wave plates in the whole working wavelength range. This device has the potential applications as a polarimeter (a rotating wave plate and a polarizer architecture with a single detector) for analyzing the state of polarization [49] or as a low cost polarization stabilizer for optimizing the performance of polarization dependent systems or devices [50].

3.5 Tunable bandpass filter

Tunable bandpass filters are extensively used as key components in fiber-optic communication and fiber-optic sensing systems. The tunability of the bandwidth represents a degree of freedom required in these applications. Many methods have been applied to achieve all-in-fiber bandpass filters, such as core mode blocker between two long-period fiber gratings [51] and acousto-optic method [52]. The presence of PCFs opens a new path for realizing all-in-fiber bandpass filters. The tuning mechanism has been proposed either by applying a thermal gradient to a PCF filled with a high index fluid [53] or by controlling the bending diameter of the splicing of solid-core PBG fiber and Bragg fiber [54]. However, the thermal gradient control is complicated and slow, and the bending manipulation can easily result in an unstable performance.

An electrically tunable bandpass filter based on two solid-core PCFs filled with different LCs is demonstrated. The tunability of the bandwidth is achieved by individually or simultaneously controlling the driving voltage of each LCPBG fiber. When two solid-core PCFs with different dimensions are filled with different LCs, the resulting transmission spectrum is the overlap of two different spectra of each LCPBG fiber, therefore forms a bandpass filter. When the driving voltage (1 kHz sine wave) of each LC filled section is changed, both the short-wavelength edge and long-wavelength edge of this bandpass filter can be tuned which is determined by the reorientation of LC molecules with respect to the applied electric field, as well as the dimension of the host fibers. The bandwidth is subsequently narrowed or enlarged depending on the direction of the bandgap edge shift. The fibers used in this work are customer designed LMA PCFs (NKT Photonics A/S, Denmark) with a solid-core surrounded by 5 rings of air-holes arranged in a triangular lattice. By using capillary forces, LC MDA-00-3969 (Merck, Germany, $n_o = 1.50$ and $n_e = 1.72$ at 589 nm) is filled in a 10 mm long PCF1 with the hole diameter and inter-hole distance of 6.02 and 9.69 μm, negative dielectric LC MLC-6884 (Merck, Germany, $n_o = 1.48$, $n_e = 1.57$ at 589 nm) is filled in a 10 mm long PCF2 with the hole diameter and inter-hole distance of 5.51 and 9.57 μm. Polarized microscopy observations on a single 5 μm LC filled capillary show that MDA-00-3969 is in a 45° splayed alignment and MLC-6884 is in a 90° splayed alignment.

Figure 8(a) shows the transmission spectra of individual LCPBG fiber used in this work. The temperature is fixed at 25°C. No voltage is applied on MDA-00-3969 filled PCF1, while 90 Vrms is applied to MLC-6884 filled PCF2. The yellow region is the overlap of two spectra in the wavelength range of 1520 – 1680 nm. Simply by tailoring the size of air-holes of each LC filled section, the spectral position of the overlapped region can be transferred to the required working wavelength range for different applications. When the driving voltage of each LCPBG fiber increases, the short-wavelength edge of MDA-00-3969 filled PCF1 is shifted toward longer wavelengths, and the long-wavelength edge of MLC-6884 filled PCF2 in the overlapped region is shifted to shorter wavelengths. Therefore, both the short-wavelength and long-wavelength edge of the formed bandpass filter can be tuned individually or simultaneously, which allows the fabrication of bandpass filter device with a continuous and flexible bandwidth control. After the filling, the two end facets of LCPBG fibers are butt-coupled and then placed in a silicon V-groove with one pair of Au electrodes deposited on the side walls of the groove, as shown in Fig. 8(b). Two SMFs are also set in the V-groove at each end of the

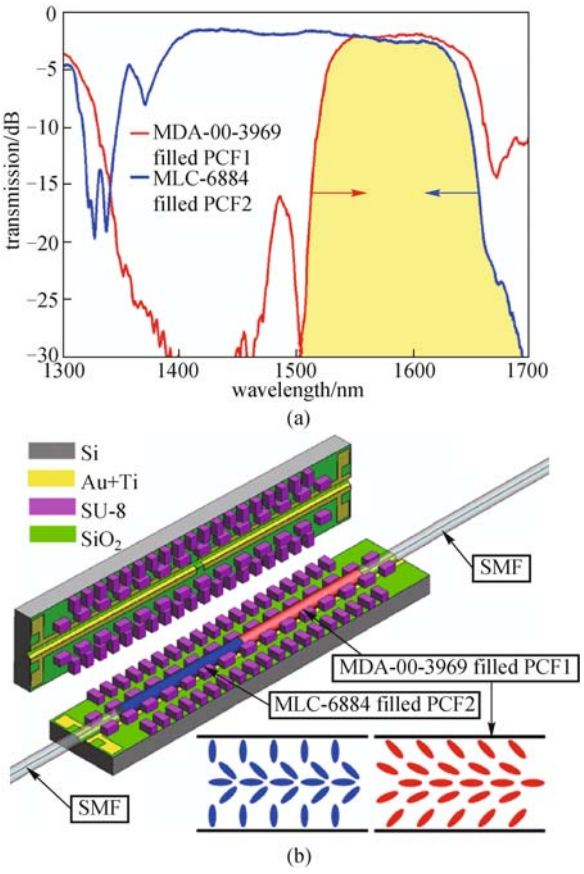

Fig. 8 (a) Transmission spectrum of individual LC filled section. The yellow region is the overlap of two spectra; (b) device assembly of the bandpass filter. MDA-00-3969 is in a 45° splayed alignment and MLC-6884 is in a 90° splayed alignment [71]

LCPBG fibers to couple the light in and out of the device. A top lid containing a V-groove with two separated pairs of electrodes is then mounted on top of the fibers and fixes the fibers in the V-grooves.

Light from a supercontinuum source (NKT Photonics A/S, Denmark) is coupled to the device and the transmission spectrum is measured by an optical spectrum analyzer and normalized to the transmission spectrum without inserting the device. Figure 9(a) shows the transmission spectra of the device when the driving voltage of MLC-6884 filled PCF2 changes and no voltage is applied to MDA-00-3969 filled PCF1. The long-wavelength edge of the filter is shifted toward shorter wavelengths by increasing the voltage, while the short-wavelength edge is kept. During the tuning process, the tunability of 3 dB bandwidth is 36 nm, when the driving voltage varies from 90 to 120 Vrms. When the driving voltage is further increased, a larger tunability can be obtained. The total insertion loss of this device is 4.7 dB at the central wavelength of 1595 nm of the filter, which is mainly contributed by the coupling losses from different interfaces in the device (air: MDA-00-3969, MDA-00-3969: MLC-6884, and MLC-6884: air), the scattering loss of LCs and a slight misalignment of SMFs and LCPBG fibers. Figure 9(b) shows the transmission spectra of the device when the driving voltage of MDA-00-3969 filled PCF1 changes and 90 Vrms is applied to MLC-6884 filled PCF2. The short-wavelength edge is shifted toward longer wavelengths by increasing the voltage and the long-wavelength edge is kept. The tunability of 3 dB bandwidth is 12 nm, when the driving voltage changes from 90 to 120 Vrms. The uneven electrical tunability between MDA-00-3969 filled PCF1 and MLC-6884 filled PCF2 is mainly caused by the different dielectric properties of LCs, and the bandgap shift is strongly connected to the reorientation of LC molecules with respect to the driving voltage. When the driving voltages of two LCPBG fibers are changed simultaneously, both the short-wavelength and long-wavelength edge can be shifted as shown in Fig. 9(c). The 3 dB bandwidth changes from 95 to 48 nm with the driving voltage varies from 90 to 120 Vrms. Weak polarization dependence is also found both for MDA-00-3969 filled PCF1 and MLC-6884 filled PCF2 working at the driving voltage below 120 Vrms.

Compared to single LC filling, this device offers more flexible bandwidth control. Considering the large number of available electrically tunable LCs and the high degree of freedom in PCF design, this compact design for LCPBG fiber based bandpass filters is a promising platform for a variety of applications, where the insertion loss and bandwidth tunability would allow for further optimization.

4 Applications

4.1 Optically fed microwave true-time delay

Microwave photonics has attracted increasing attention for processing microwave and millimeter-wave signals directly in the optical domain [55]. One important application is the true-time delay based on photonic technologies, which is an effective way to realize broadband phased array systems [56]. The reported techniques can be classified into two categories: active optical devices, such as active semiconductor waveguides using coherent population oscillation [57] or optical fiber using stimulated Brillouin scattering [58], and passive optical devices [59–64]. In general, the true-time delay based on passive optical devices is mostly realized by exploring waveguide dispersion through time-domain phase shift method, which detects the phase of light sinusoidally modulated at gigahertz frequencies [56]. Among the proposed approaches, fiber grating devices, as a well-developed one-dimensional periodic structure, still play an important role in designing compact and reliable true-time delay units [59]. A minimum broadband true-time delay of 1 ps at up to 30 GHz based on a linearly chirped fiber Bragg grating has been analyzed either by changing the temperature or strain along the grating region [60].

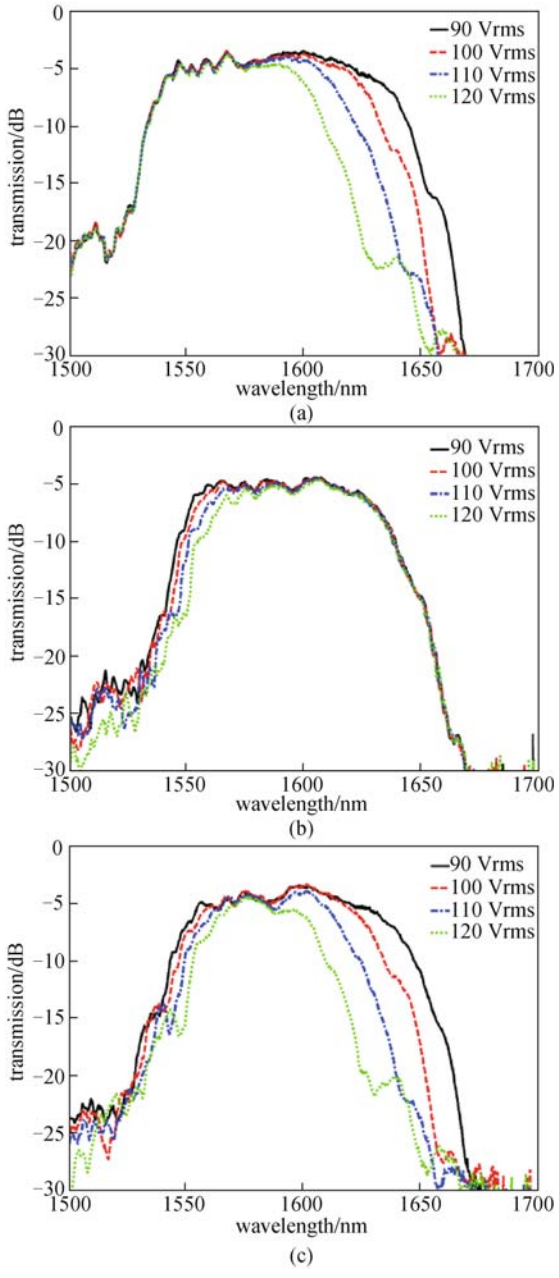

Fig. 9 (a) Transmission spectra of the device when the driving voltage of MLC-6884 filled PCF2 changes and no voltage is applied to MDA-00-3969 filled PCF1; (b) transmission spectra of the device when the driving voltage of MDA-00-3969 filled PCF1 changes and 90 Vrms is applied to MLC-6884 filled PCF2; (c) transmission spectra of the device when the driving voltages of two LCPBG fibers are changed simultaneously [71]

Meanwhile, progress in two-dimensional photonic crystal waveguides (PCWs) reveals a promising solution for buffering and time-domain processing of optical signal by tailoring the dispersion properties. A rapid increase in group index up to several tens is observed near the bandgap edge [61]. At present, solutions to control the group velocity are mainly based on local heating [62] or microfluidic infiltration [63]. However, the transmission loss in PCWs (typically 20 dB transmission drop near bandgap edge for a 200 μm long device [61,62]) is also a challenge and required to be conquered in practical applications. Moreover, PBG fibers, which confine light using bandgap effects by two-dimensional periodic cladding, have also been employed in the true-time delay modules. A continuously tunable time delay from 0 to 500 ps over 1 GHz bandwidth at X-band has been demonstrated with a broadband light source through a 20.13 m long PBG fiber [64]. PBG fibers improve the stability and integratability of true-time delay module. Nevertheless, external precisely broadband optical tunable filters are required. The development of electrically driven LCPBG fiber devices indicates that LC as an infiltration candidate provides the attractive basis for externally tuning the group index of waveguide.

The fiber used in the experiments is LMA-13 (NKT Photonics A/S, Denmark) and the LC is MDA-00-3969 (Merck, Germany). Figure 10(a) shows the transmission bandgap in the wavelength range 1300–1600 nm with different driving voltages at 23°C. It is evident that the short-wavelength edge is shifted toward longer wavelengths by increasing the driving voltage. Figure 10(b) describes the experimental setup to measure the RF phase shift or time delay in the LCPBG fiber device. The electrical microwave signal is generated by the network

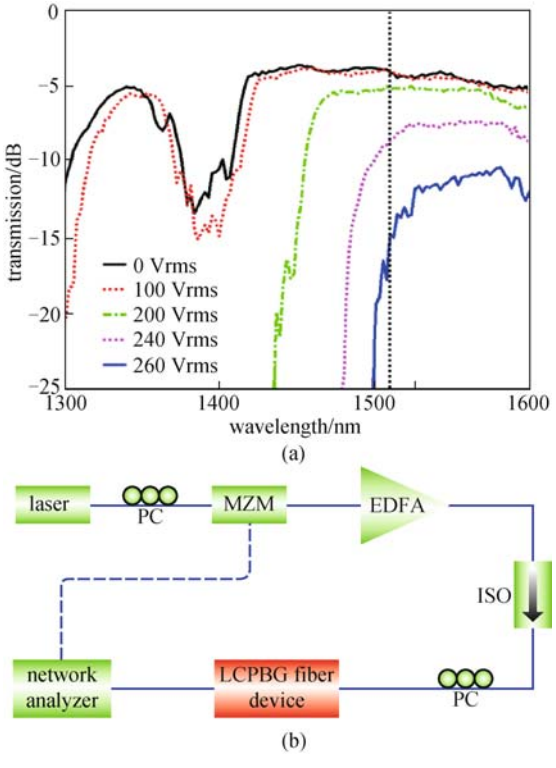

Fig. 10 (a) Transmission spectrum of the LCPBG fiber device with different applied voltages. The black dotted line is the optical carrier at 1510 nm used in experiments; (b) experimental setup for investigating the RF phase shift or time delay in the LCPBG fiber device [72]

analyzer, and modulated by a Mach-Zehnder modulator (MZM) onto a laser beam with the wavelength of 1510 nm, shown as the black dotted line in Fig. 10(a). The modulated optical signal is coupled into the integrated LCPBG fiber device, and then converted back to electrical microwave signal by a high speed photo detector inside the network analyzer. The network analyzer compares the received signal with the internal reference and infers the microwave phase shift and corresponding power change. An erbium-doped fiber amplifier (EDFA) is used to control the input optical power to the device, and the polarization state of the input beam is selected by polarization controllers (PCs).

Figure 11(a) shows the measured RF phase shift and the relative RF power change as a function of the driving voltage for different modulation frequencies, respectively. The results demonstrate a continuously tunable RF phase shifter by changing the driving voltage. A maximum RF phase shift of around 70° at a modulation frequency of 15 GHz is achieved. An obvious phase shift for different modulation frequencies is observed only when the driving voltage is higher than 220 Vrms. Since the short-wavelength bandgap edge starts to cross 1510 nm above 220 Vrms, a distinct change of group index at this wavelength is expected. Figure 11(b) shows the RF phase shift and corresponding time delay as a function of the modulation frequency. The value of group index change is 0.071 at 240 Vrms, 0.113 at 250 Vrms and 0.194 at 260 Vrms. At 260 Vrms, an averaged 12.9 ps time delay over the whole measurement bandwidth is achieved, which indicates a broadband microwave true-time delay. If the driving voltage increases further, a longer time delay will be expected. However, a larger power decrease has to be considered. One possible solution is to combine optical amplifiers as power boosters. The maximum modulation frequency here is only limited by the capacity of the network analyzer. The large RF phase variations at high frequencies around 15 GHz are mainly caused by the electrical modulation signal out of the operating range of network analyzer. Furthermore, the signal quality could be largely improved by diminishing the mismatch between the bandgap position of the device and the optimal working wavelength range of EDFA and the modulator.

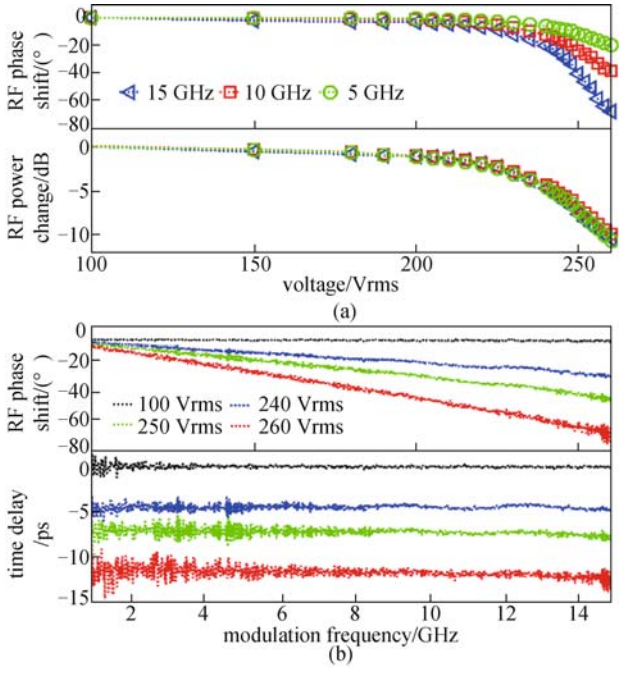

Fig. 11 (a) RF phase shift and relative RF power change as a function of the driving voltage for different modulation frequencies; (b) RF phase shift and corresponding time delay as a function of the modulation frequency for different driving voltages [72]

4.2 Electrically tunable Yb-doped fiber laser

Using the wavelength filtering effect of PBG confinement with an Yb-doped core has previously been used in solid-core PBG fiber lasers and amplifiers. The bandgap efficiently suppresses the amplified spontaneous emission (ASE) at the conventional ytterbium gain wavelengths around 1030 nm and enables both short [65] and long wavelength operation [66]. The PBG fiber laser concept with the tunability offered by LCs has been combined to create an all-spliced fiber laser with a single-mode output and electrical tunability in the range 1040 – 1065 nm. The presence of a bandgap in the laser cavity inhibits lasing at certain wavelengths, thus by applying an electric field to an intra-cavity LCPBG fiber the bandgap position can be shifted, resulting in laser tunability. The device holds potential as a low cost tunable seed source for ytterbium fiber amplifiers.

The fiber used in the experiments is LMA-13 (NKT Photonics A/S, Denmark), and the LC is MDA-00-3969 (Merck, Germany). As shown in Fig. 12, the all-spliced fiber assembly is comprised of the integrated LCPBG fiber device, an Yb-doped airclad PCF, a pump diode and a 6 + 1:1 pump/signal combiner for airclad fibers with polarization-maintaining (PM) single mode signal feed-through. The combiner is designed for 0.15 NA pump diodes, and in order to utilize the high NA supported by airclad fibers, it features a special taper element [67]. An illustration of the combiner is shown in the bottom right inset of Fig. 12. The 7 input fibers have an outer diameter of 125 μm. The pump fibers have a core diameter of 105 μm and the signal fiber is a single mode PM fiber with a mode field diameter of 10.5 μm. The 7 input fibers are fused together into a fiber bundle with the SMF in the center and spliced to the input end of a taper element. The output end of the taper element is then spliced to a passive double-clad delivery fiber. The laser cavity is formed by a lens and silver mirror after the integrated LCPBG fiber device and the cleaved end facet of the ytterbium-doped PCF with a pump cladding diameter

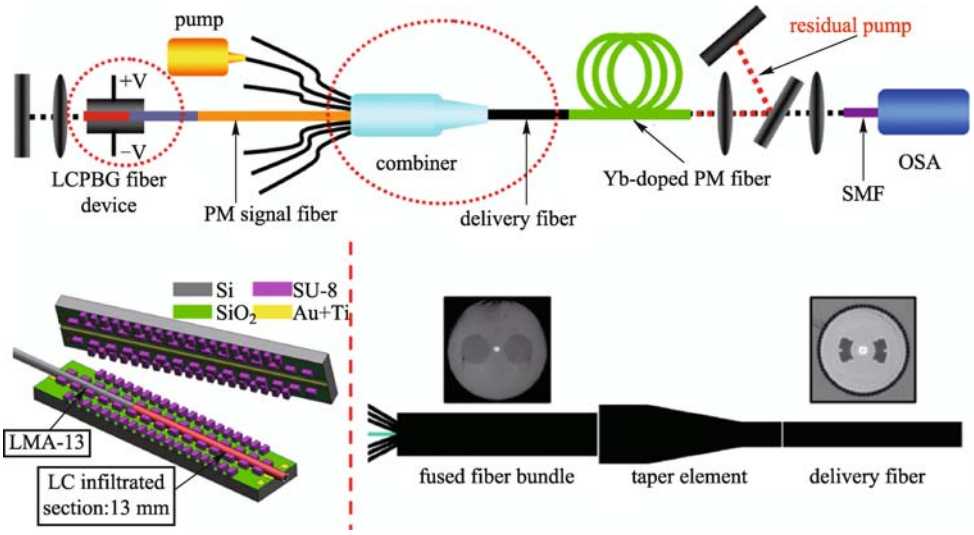

Fig. 12 All-spliced laser cavity setup from the left: cavity mirror, LCPBG fiber device, pump/signal combiner with single-mode signal feed-through, Yb-doped PCF, long wave pass filter, and OSA. Bottom left: the assembly of LCPBG fiber device. Bottom right: schematic of 6+1:1 pump/signal combiner [73]

of 105 μm and a mode field diameter of 12 μm. With a pump absorption of 3 dB/m and a length of 4 m it is optimized for 976 nm pumping. The residual pump is filtered by a long wave pass filter at the output of the laser cavity while the laser signal spectrum is recorded by an optical spectrum analyzer.

In PBG fiber lasers, lasing occurs at the wavelengths that experience the least loss due to the bandgap combined with the highest gain caused by their emission cross section. These wavelengths are close to the short wavelength edge of the bandgap. Fiber lasers based on active PBG fibers typically have distributed spectral filtering along the whole length of the fiber in order to reduce ASE, whereas in the LCPBG device the LC infiltrated section is only 13 mm long. Hence, ASE will inevitably build up in the Yb-doped fiber, resulting in parasitic lasing which will limit the tunability and power scalability of the LCPBG fiber laser. Figures 13(a)–13(c) show the laser transmission spectra compared to the bandgap transmission spectra for three different voltage setting, 0, 150 and 160 Vrms. For low voltages the ASE peak is well inside the bandgap and therefore tuning of the bandgap edge does not affect the lasing wavelength significantly. For higher voltages the ASE peak is outside the bandgap, while the laser wavelength is tuned inside the bandgap. For voltages of 160 Vrms and higher, the loss inside the bandgap becomes too high leading to parasitic lasing outside the bandgap. Figure 13(d) plots the narrow laser spectra of the cavity for different voltage settings. The laser wavelength is shifted toward longer wavelengths by approximately 25 nm. The wavelength is constant at 1040 nm below 130 Vrms and tunable up to 1065 nm at 155 Vrms.

The laser cavity produces an output of around 30 mW with the efficiency of the laser strongly limited by losses in the cavity. With optimization of cavity optics, fiber cleave angles, LC device, and mode matching between fibers, losses can be reduced and potentially allow for the production of an easily tunable, single mode output signal, which can be used to seed a fiber amplifier. The present cavity yields up to 25 dB of ASE suppression, however an improved cavity with reflectors in both ends is expected to improve the ASE suppression significantly. With improvements to the system, the device holds potential as a low cost, compact and easy-to-use tunable seed source for fiber amplifiers.

5 Conclusions

The interesting properties and useful characteristics of the integrated LCPBG fiber devices show a promising future focused on applications of these LCPBG devices in real systems [68–75]. For fundamental features, a better understanding of the alignment of LCs in silica capillary is required to have a clearer picture of the physics behind LCs contained in cylindrical geometries. Combining this with improved surface coating techniques to control the pre-tilt angles could yield electrically controlled devices requiring lower driving voltage. Simulations could be improved by including scattering and absorption into the model and by implementing methods that can simulate index variation along the third direction, for example a beam propagation method. From application point of view, more system experiments need to be carried out in order to demonstrate the potential value of this technology in real applications.

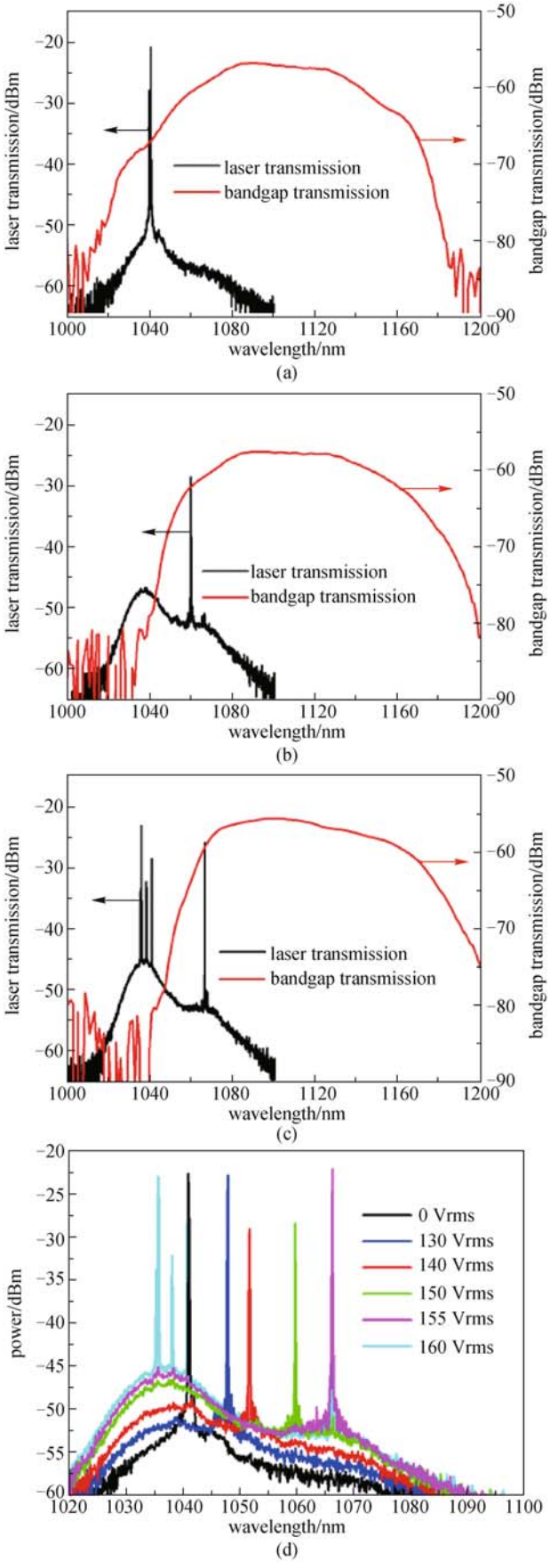

Fig. 13 Laser transmission spectra compared to bandgap transmission spectra for (a) 0 Vrms, (b) 150 Vrms, and (c) 160 Vrms; (d) laser spectra of the cavity for different applied voltages [73]

Acknowledgements We are grateful to T. T. Alkeskjold, J. Weirich, L. Scolari, W. Xue, Y. Chen, C. B. Olausson, D. Noordegraaf, L. Eskildsen, J. Laegsgaard and A. Bjarklev for fruitful collaboration and discussion. This work was supported in part by the Singapore Ministry of Education Academic Research Fund Tier 2 (MOE2015-T2-1-066), MINDEF-NTU-JPP/15/01/02, and Nanyang Technological University (Startup grant: Lei Wei).

References

1. Knight J C, Birks T A, Russell P S J, Atkin D M. All-silica single-mode optical fiber with photonic crystal cladding. Optics Letters, 1996, 21(19): 1547–1549
2. Bjarklev A, Broeng J, Bjarklev A S. Photonic Crystal Fibres. Boston, MA: Kluwer Academic Publishers, 2003
3. Russell P S J. Photonic crystal fibers. science, 2003, 299(5605): 358–362
4. Bise R T, Windeler R S, Kranz K S, Kerbage C, Eggleton B J, Trevor D J. Tunable photonic band gap fiber. In: Proceedings of Optical Fiber Communication Conference and Exhibit, 2002. Anaheim: IEEE, 2002, 466–468
5. Larsen T, Bjarklev A, Hermann D, Broeng J. Optical devices based on liquid crystal photonic bandgap fibres. Optics Express, 2003, 11 (20): 2589–2596
6. Agrawal G P. Fiber-Optic Communication Systems. New York: John Wiley & Sons, 2012
7. Green M, Madden S J. Low loss nematic liquid crystal cored fiber waveguides. Applied Optics, 1989, 28(24): 5202–5203
8. Lorenz A, Schuhmann R, Kitzerow H S. Infiltrated photonic crystal fiber: experiments and liquid crystal scattering model. Optics Express, 2010, 18(4): 3519–3530
9. Du F, Lu Y Q, Wu S T. Electrically tunable liquid-crystal photonic crystal fiber. Applied Physics Letters, 2004, 85(12): 2181–2183
10. Haakestad M W, Alkeskjold T T, Nielsen M D, Scolari L, Riishede J, Engan H E, Bjarklev A. Electrically tunable photonic bandgap guidance in a liquid-crystal-filled photonic crystal fiber. IEEE Photonics Technology Letters, 2005, 17(4): 819–821
11. Scolari L, Alkeskjold T, Riishede J, Bjarklev A, Hermann D, Anawati A, Nielsen M, Bassi P. Continuously tunable devices based on electrical control of dual-frequency liquid crystal filled photonic bandgap fibers. Optics Express, 2005, 13(19): 7483–7496
12. Wei L, Eskildsen L, Weirich J, Scolari L, Alkeskjold T T, Bjarklev A. Continuously tunable all-in-fiber devices based on thermal and electrical control of negative dielectric anisotropy liquid crystal photonic bandgap fibers. Applied Optics, 2009, 48(3): 497–503
13. Cognard J. Alignment of Nematic Liquid Crystals and Their Mixtures-Molecular Crystals and Liquid Crystals Supplement Series. London, New York: Gordon and Breach Science Publishers, 1982
14. Anawati A. Alignment in cylindrical geometry and dielectric properties. Dissertation for the Master Degree. Sweden: Chalmers University of Tecnhology, 2005
15. Lorenz A, Kitzerow H S, Schwuchow A, Kobelke J, Bartelt H. Photonic crystal fiber with a dual-frequency addressable liquid crystal: behavior in the visible wavelength range. Optics Express, 2008, 16(23): 19375–19381
16. Litchinitser N, Dunn S, Steinvurzel P, Eggleton B, White T, McPhedran R, de Sterke C. Application of an ARROW model for designing tunable photonic devices. Optics Express, 2004, 12(8): 1540–1550
17. Lægsgaard J. Gap formation and guided modes in photonic bandgap fibres with high-index rods. Journal of Optics A, Pure and Applied Optics, 2004, 6(8): 798–804
18. Ren G, Shum P, Hu J, Yu X, Gong Y. Polarization-dependent bandgap splitting and mode guiding in liquid crystal photonic bandgap fibers. Journal of Lightwave Technology, 2008, 26(22): 3650–3659
19. Hu J J, Ren G, Shum P, Yu X, Wang G, Lu C. Analytical method for band structure calculation of photonic crystal fibers filled with liquid crystal. Optics Express, 2008, 16(9): 6668–6674
20. Weirich J, Laegsgaard J, Wei L, Alkeskjold T T, Wu T X, Wu S T, Bjarklev A. Liquid crystal parameter analysis for tunable photonic bandgap fiber devices. Optics Express, 2010, 18(5): 4074–4087
21. Duguay M, Kokubun Y, Koch T L, Pfeiffer L. Antiresonant reflecting optical waveguides in SiO_2-Si multilayer structures. Applied Physics Letters, 1986, 49(1): 13–15
22. Litchinitser N M, Abeeluck A K, Headley C, Eggleton B J. Antiresonant reflecting photonic crystal optical waveguides. Optics Letters, 2002, 27(18): 1592–1594
23. Litchinitser N M, Dunn S C, Usner B, Eggleton B J, White T P, McPhedran R C, de Sterke C M. Resonances in microstructured optical waveguides. Optics Express, 2003, 11(10): 1243–1251
24. Litchinitser N, Poliakov E. Antiresonant guiding microstructured optical fibers for sensing applications. Applied Physics. B, Lasers and Optics, 2005, 81(2–3): 347–351
25. Alkeskjold T T. Optical devices based on liquid crystal photonic bandgap fibers. Dissertation for the Doctoral Degree. DKongens Lyngby: Technical University of Denmark, 2005
26. Noordegraaf D, Scolari L, Laegsgaard J, Tanggaard Alkeskjold T, Tartarini G, Borelli E, Bassi P, Li J, Wu S T. Avoided-crossing-based liquid-crystal photonic-bandgap notch filter. Optics Letters, 2008, 33(9): 986–988
27. Hu C, Whinnery J R. Losses of a nematic liquid-crystal optical waveguide. JOSA, 1974, 64(11): 1424–1432
28. Ferrarini D, Vincetti L, Zoboli M, Cucinotta A, Selleri S. Leakage properties of photonic crystal fibers. Optics Express, 2002, 10(23): 1314–1319
29. Alkeskjold T T, Bjarklev A. Electrically controlled broadband liquid crystal photonic bandgap fiber polarimeter. Optics Letters, 2007, 32 (12): 1707–1709
30. Wei L, Alkeskjold T T, Bjarklev A. Compact design of an electrically tunable and rotatable polarizer based on a liquid crystal photonic bandgap fiber. IEEE Photonics Technology Letters, 2009, 21(21): 1633–1635
31. Vengsarkar A M, Lemaire P J, Judkins J B, Bhatia V, Erdogan T, Sipe J E. Long-period fiber gratings as band-rejection filters. Journal of Lightwave Technology, 1996, 14(1): 58–65
32. Vengsarkar A M, Pedrazzani J R, Judkins J B, Lemaire P J, Bergano N S, Davidson C R. Long-period fiber-grating-based gain equalizers. Optics Letters, 1996, 21(5): 336–338
33. Poole C D, Wiesenfeld J M, Digiovanni D J, Vengsarkar A M. Optical fiber-based dispersion compensation using higher order modes near cutoff. Journal of Lightwave Technology, 1994, 12(10):

1746–1758
34. Bhatia V, Vengsarkar A M. Optical fiber long-period grating sensors. Optics Letters, 1996, 21(9): 692–694
35. Rindorf L, Jensen J B, Dufva M, Pedersen L H, Høiby P E, Bang O. Photonic crystal fiber long-period gratings for biochemical sensing. Optics Express, 2006, 14(18): 8224–8231
36. Kakarantzas G, Birks T A, Russell P S J. Structural long-period gratings in photonic crystal fibers. Optics Letters, 2002, 27(12): 1013–1015
37. Morishita K, Miyake Y. Fabrication and resonance wavelengths of long-period gratings written in a pure-silica photonic crystal fiber by the glass structure change. Journal of Lightwave Technology, 2004, 22(2): 625–630
38. Lim J H, Lee K S, Kim J C, Lee B H. Tunable fiber gratings fabricated in photonic crystal fiber by use of mechanical pressure. Optics Letters, 2004, 29(4): 331–333
39. Brambilla G, Fotiadi A A, Slattery S A, Nikogosyan D N. Two-photon photochemical long-period grating fabrication in pure-fused-silica photonic crystal fiber. Optics Letters, 2006, 31(18): 2675–2677
40. Yeom D I, Steinvurzel P, Eggleton B J, Lim S D, Kim B Y. Tunable acoustic gratings in solid-core photonic bandgap fiber. Optics Express, 2007, 15(6): 3513–3518
41. Noordegraaf D, Scolari L, Lægsgaard J, Rindorf L, Alkeskjold T T. Electrically and mechanically induced long period gratings in liquid crystal photonic bandgap fibers. Optics Express, 2007, 15(13): 7901–7912
42. de Gennes P G. The Physics of Liquid Crystals. New York: Oxford University Press, 1993
43. Ulrich R. Polarization stabilization on single-mode fiber. Applied Physics Letters, 1979, 35(11): 840–842
44. Imai T, Nosu K, Yamaguchi H. Optical polarisation control utilising an optical heterodyne detection scheme. Electronics Letters, 1985, 21(2): 52–53
45. Heismann F. Integrated-optic polarization transformer for reset-free endless polarization control. IEEE Journal of Quantum Electronics, 1989, 25(8): 1898–1906
46. Rumbaugh S H, Jones M D, Casperson L W. Polarization control for coherent fiber-optic systems using nematic liquid crystals. Journal of Lightwave Technology, 1990, 8(3): 459–465
47. Kerbage C, Eggleton B. Numerical analysis and experimental design of tunable birefringence in microstructured optical fiber. Optics Express, 2002, 10(5): 246–255
48. Knape H, Margulis W. All-fiber polarization switch. Optics Letters, 2007, 32(6): 614–616
49. Azzam R M. Poincaré sphere representation of the fixed-polarizer rotating-retarder optical system. Journal of the Optical Society of America A, Optics, Image Science, and Vision, 2000, 17(11): 2105–2107
50. Chiba T, Ohtera Y, Kawakami S. Polarization stabilizer using liquid crystal rotatable waveplates. Journal of Lightwave Technology, 1999, 17(5): 885–890
51. Starodubov D, Grubsky V, Feinberg J. All-fiber bandpass filter with adjustable transmission using cladding-mode coupling. IEEE Photonics Technology Letters, 1998, 10(11): 1590–1592
52. Yeom D I, Kim H S, Kang M S, Park H S, Kim B Y. Narrow-bandwidth all-fiber acoustooptic tunable filter with low polarization-sensitivity. IEEE Photonics Technology Letters, 2005, 17(12): 2646–2648
53. Steinvurzel P, Eggleton B, de Sterke C M, Steel M. Continuously tunable bandpass filtering using high-index inclusion microstructured optical fibre. Electronics Letters, 2005, 41(8): 463–464
54. Liu B W, Hu M L, Fang X H, Li Y F, Chai L, Li J Y, Chen W, Wang C Y. Tunable bandpass filter with solid-core photonic bandgap fiber and Bragg fiber. IEEE Photonics Technology Letters, 2008, 20(8): 581–583
55. Seeds J, Williams K J. Microwave photonics. Journal of Lightwave Technology, 2006, 24(12): 4628–4641
56. Yao J. Microwave photonics. Journal of Lightwave Technology, 2009, 27(3): 314–335
57. Öhman F, Yvind K, Mørk J. Slow light in a semiconductor waveguide for true-time delay applications in microwave photonics. IEEE Photonics Technology Letters, 2007, 19(15): 1145–1147
58. Okawachi Y, Bigelow M S, Sharping J E, Zhu Z, Schweinsberg A, Gauthier D J, Boyd R W, Gaeta A L. Tunable all-optical delays via Brillouin slow light in an optical fiber. Physical Review Letters, 2005, 94(15): 153902
59. Edge C, Molony A, Bennion I. Fibre grating time delay element for phased array antennas. Electronics Letters, 1995, 31(17): 1485–1486
60. Italia V, Pisco M, Campopiano S, Cusano A, Cutolo A. Chirped fiber Bragg gratings for electrically tunable time delay lines. IEEE Journal of Selected Topics in Quantum Electronics, 2005, 11(2): 408–416
61. Baba T. Slow light in photonic crystals. Nature Photonics, 2008, 2 (8): 465–473
62. Vlasov Y A, O'Boyle M, Hamann H F, McNab S J. Active control of slow light on a chip with photonic crystal waveguides. Nature, 2005, 438(7064): 65–69
63. Ebnali-Heidari M, Grillet C, Monat C, Eggleton B J. Dispersion engineering of slow light photonic crystal waveguides using microfluidic infiltration. Optics Express, 2009, 17(3): 1628–1635
64. Liu Z, Zheng X, Zhang H, Guo Y, Zhou B. X-band continuously variable true-time delay lines using air-guiding photonic bandgap fibers and a broadband light source. Optics Letters, 2006, 31(18): 2789–2791
65. Pureur V, Bigot L, Bouwmans G, Quiquempois Y, Douay M, Jaouen Y. Ytterbium-doped solid core photonic bandgap fiber for laser operation around 980 nm. Applied Physics Letters, 2008, 92 (6): 061113
66. Shirakawa A, Maruyama H, Ueda K, Olausson C B, Lyngsø J K, Broeng J. High-power Yb-doped photonic bandgap fiber amplifier at 1150–1200 nm. Optics Express, 2009, 17(2): 447–454
67. Noordegraaf D, Nielsen M D, Skovgaard P M, Agger S, Hansen K P, Broeng J, Jakobsen C, Simonsen H R, Laegsgaard J. Pump combiner for air-clad fiber with PM single-mode signal feed-through. In: Proceedings of Conference on Lasers and Electro-Optics/ International Quantum Electronics Conference, CLEO2009. Baltimore: Optical Society of America, 2009, 523–524
68. Wei L, Khomtchenko E, Alkeskjold T T, Bjarklev A. Photolitho-

graphy of thick photoresist coating for electrically controlled liquid crystal photonic bandgap fibre devices. Electronics Letters, 2009, 45 (6): 326–327
69. Wei L, Weirich J, Alkeskjold T T, Bjarklev A. On-chip tunable long-period grating devices based on liquid crystal photonic bandgap fibers. Optics Letters, 2009, 34(24): 3818–3820
70. Wei L, Alkeskjold T T, Bjarklev A. Tunable and rotatable polarization controller using photonic crystal fiber filled with liquid crystal. Applied Physics Letters, 2010, 96(24): 241104
71. Wei L, Alkeskjold T T, Bjarklev A. Electrically tunable bandpass filter using solid-core photonic crystal fibers filled with multiple liquid crystals. Optics Letters, 2010, 35(10): 1608–1610
72. Wei L, Xue W, Chen Y, Alkeskjold T T, Bjarklev A. Optically fed microwave true-time delay based on a compact liquid-crystal photonic-bandgap-fiber device. Optics Letters, 2009, 34(18): 2757–2759
73. Olausson C B, Scolari L, Wei L, Noordegraaf D, Weirich J, Alkeskjold T T, Hansen K P, Bjarklev A. Electrically tunable Yb-doped fiber laser based on a liquid crystal photonic bandgap fiber device. Optics Express, 2010, 18(8): 8229–8238
74. Stolyarov A M, Wei L, Shapira O, Sorin F, Chua S L, Joannopoulos J D, Fink Y. Microfluidic directional emission control of an azimuthally polarized radial fibre laser. Nature Photonics, 2012, 6 (4): 229–233
75. Stolyarov A M, Wei L, Sorin F, Lestoquoy G, Joannopoulos J D, Fink Y. Fabrication and characterization of fibers with built-in liquid crystal channels and electrodes for transverse incident-light modulation. Applied Physics Letters, 2012, 101(1): 011108

Kaiwei Li received his B.E. degree in mechanical engineering from Jilin University, Changchun, China, in 2009, and Ph.D. degree in mechanical engineering from the Changchun Institute of Optics, Fine Mechanics and Physics (CIOMP), Chinese Academy of Sciences, Changchun, China, in 2014. Now he is a Research Fellow in School of Electrical and Electronic Engineering, Nanyang Technological University, Singapore. His research interest includes optical micro/nanofiber biochemical sensors, optical fiber SPR sensors and mid-IR fiber sensors. He is now working on novel mid-IR fiber sensors for biochemical applications.

Ting Zhang is currently a Research Fellow in School of Electrical and Electronic Engineering, Nanyang Technological University, Singapore. He received his B.E. degree in materials science and engineering from Xi'an University of Technology, China, in 2009, and Ph.D. degree in condensed matter physics from Beijing Normal University, China, in 2014. After that, he had been a Research Fellow for one year at Institute of Electrical Engineering, Chinese Academy of Sciences. His research interests focus on photonics, optoelectronic, thermoelectric and thermal transport based on nanostructures and nanomaterials, and flexible devices for energy harvest and storage.

Nan Zhang received her B.S. degree from Northwestern Polytechnical University, Xi'an, China, in 2012. She is currently working toward the Ph.D. degree in School of Electrical and Electronic Engineering, Nanyang Technological University, Singapore. Her main research interest is to develop specialty optical fiber based surface enhanced Raman scattering sensing platforms.

Mengying Zhang is a Ph.D. student of School of Electrical and Electronic Engineering at Nanyang Technological University (NTU). She received her B. Eng. degree in 2014 from NTU with First Class Honors Degree. She began Ph.D. study in August 2014. Her research area is in miniaturized sensing devices based on optical fibers. Her current work is on optical fiber based surface plasmon resonance sensors.

Jing Zhang received her B.S. degree in optoelectronics engineering from Huazhong University of Science and Technology (HUST), China, in 2012. She received the Master degree in information system and technology from Université Paris-Sud and Supélec, France, in 2014. She is currently working toward the Ph.D. degree in School of Electrical and Electronic Engineering at Nanyang Technological University, Singapore. Her current project includes the thermal and scalable fabrication of in-fiber multi-material microspheres based on microfluidics and fiber biosensor based on whispering gallery mode in active microspheres.

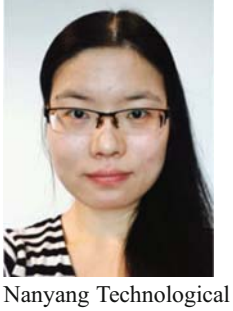

Tingting Wu received her Master degree in electronic and information engineering from Harbin Institute of Technology, China, in 2014. From 2013 to 2014, she was with School of Electrical and Electronic Engineering, Nanyang Technological University, Singapore, as an exchange student. She is now a Ph.D. student in School of Electrical and Electronic Engineering, Nanyang Technological University, Singapore. Her current research interests include silicon photonics, nonlinear optics and 2D materials based device.

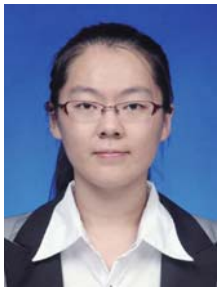

Shaoyang Ma received her B.S. degree in electronic science and technology and M.S. degree in physical electronics from Harbin Institute of Technology in 2012 and 2014, respectively. Since January 2015, she has been a Ph.D. student in School of Electrical and Electronic Engineering, Nanyang Technological University, Singapore. Her research interests lies in multi-fuctional and multi-material micro- and nano-fibers including but not limited to thermoelectric and piezoelectric fibers fabricated by electrospinning method.

Junying Wu received her B.E. degree in safety engineering from Shenyang Institute of Aeronautical Engineering, China. Now she is a project officer in School of Electrical and Electronic Engineering, Nanyang Technological University, Singapore. Her research interest includes optical micro/nanofiber, biochemical sensors. She is now working on novel mid-IR fiber sensors for biochemical application.

Ming Chen received his B.E. degree in information science from Shandong University, Jinan, China, in 2009 and Ph.D. degree in electronic science and technology from Xiamen University, Xiamen, China, in 2014. From 2014 to 2015, he was a postdoctoral fellow in Northwestern University, Evanston, USA. He is currently a Research Fellow with School of Electrical and Electronic Engineering, Nanyang Technological University, Singapore. His research interests include III-nitride semiconductor lasers, vertical cavity surface emitting lasers, light emitting diodes, InP-based quantum cascade lasers and fiber devices.

Yi He received his M.S. degree in 2009 at Southwest University of Science and Technology, China. He completed his Ph.D. in 2014 at University of Science and Technology of China. In 2015, he joined the School of Electrical and Electronic Engineering at Nanyang Technological University in Singapore as a research fellow. His current research interests are focused on the construction of multifunctional optical fiber devices and their biological applications.

Lei Wei received his B.E. degree in electrical engineering from Wuhan University of Technology, China, in 2005; and Ph. D. degree in photonics engineering from Technical University of Denmark, Denmark, in 2010. Then he joined the Massachusetts Institute of Technology as a postdoctoral associate. In 2014, he joined the School of Electrical and Electronic Engineering at Nanyang Technological University in Singapore as a Nanyang Assistant Professor. His main research interests are fiber-based optoelectronic devices, multimaterial fibers, bio-fiber interfaces, and in-fiber energy generation and storage.